# A WAVE MODELLING STUDY OF AN INTENSE STORM IN BASS STRAIT, AUSTRALIA

Diana J. M. Greenslade

Bureau of Meteorology Research Centre
Melbourne, VIC, Australia

## 1. INTRODUCTION

This paper describes a case study of a storm which passed over the Bass Strait area (see Figure 1) during December 1998. This particular storm attracted much media attention due to the fact that it devastated the fleet of the 1998 Sydney to Hobart yacht race. This race turned out to be the most disastrous event in the race's 54-year history, and indeed of any offshore race in Australian waters. Of the 115 yachts departing Sydney Harbour at 1pm on December 26th, only 44 reached their destination. Sixty-six boats retired from the race and five were lost completely. Tragically, six people lost their lives during the storm and another fifty-five people were rescued in the biggest maritime rescue operation ever undertaken in Australian waters (Cruising Yacht Club of Australia, 1999, hereafter CYC99).

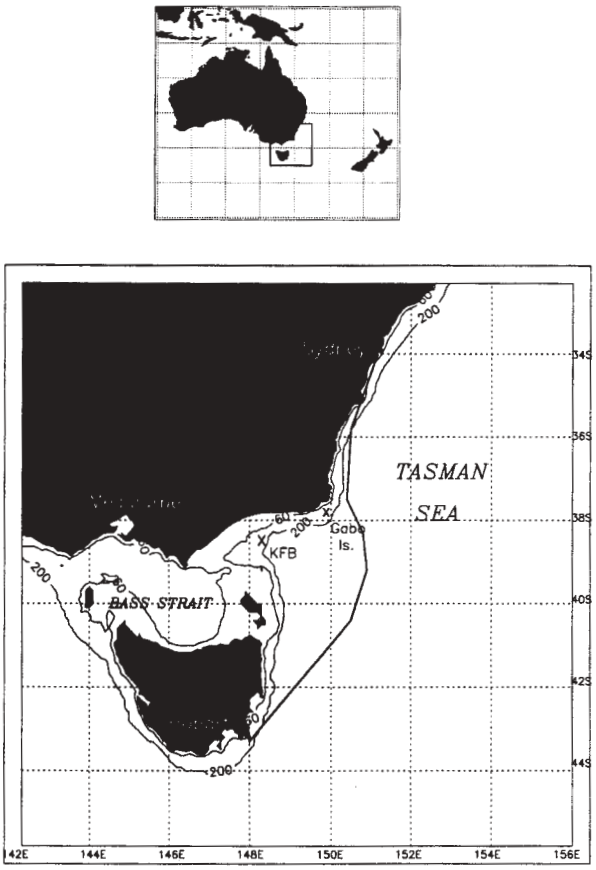


**Figure 1. This map shows the area of the Sydney to Hobart yacht race. 60m and 200m bathymetric depth contours are marked. The thick black line shows the trajectory taken by one of the yachts to complete the race.**

Figure 1 shows a map of the race region with a few depth contours outlined. The thick line on this figure represents the trajectory taken by one of the 44 yachts to finish the race. It can be seen that after reaching Gabo Island, the yacht was subsequently blown off course by the storm. Also marked on the map is Kingfish B oil platform (KFB), from which marine observations were available.

The aim of this paper is to examine the evolving sea-state during the yacht race. Section 2 describes the wave model and wind forcing fields used for this study. The modelled wave fields are described in Section 3, along with a discussion of some potentially important factors governing the development of the sea-state. In Section 4, the surface winds and wave model results are compared with the available observations and possible causes for discrepancies are discussed, and Section 5 presents the conclusions.

## 2. DESCRIPTION OF THE WAVE MODEL

The wave model used for this study is a high-resolution version of the wave model, WAM. The WAM model (Komen *et al.*, 1994) is a third generation wave model, i.e., the wave transport equation is solved explicitly without assuming a form for the evolving wave spectrum. The wave transport equation is:

$$\frac{\partial F}{\partial t} + \nabla\left(c_g F\right) = S_{in} + S_{nl} + S_d + S_{bot} \qquad (1)$$

where $F$ is the wave spectrum, $c_g$ is the group velocity and the terms on the right hand side represent the source terms: $S_{in}$ is the energy input due to wind forcing, $S_{nl}$ the non-linear energy transfer between groups of resonant waves, $S_d$ the dissipation of energy due to whitecapping, and $S_{bot}$ the dissipation of energy due to bottom friction. The WAM model is implemented operationally at many forecasting centres around the world, including a version at the Australian Bureau of Meteorology (AUSWAM).

AUSWAM currently comprises a global model at 3° spatial resolution, a regional model at 1° resolution and a mesoscale model at 0.25° resolution. The mesoscale model is nested inside the regional model, which is in turn nested inside the global model. The regional model spans the oceans around Australia and covers an area from 60°S to 12°N and from 69°E to 180°. The mesoscale model covers the southeast of Australia and ranges from 50°S to 24°S and from 126°E to 164°E.

For the global and regional models the source terms are integrated every 10 minutes and the propagation terms every 20 minutes, while for the mesoscale model, the timestep is 5 minutes for both source and propagation terms. In terms of the wave spectrum, the directional resolution is 30° and there are 25 frequency bins ranging from 0.0418 Hz to 0.4114 Hz. This represents wave periods from approximately 24 seconds to 2.5 seconds. At spatial resolutions of 1° or greater, very few of the wave model gridpoints are in water depths of less than 100m and so the regional and global wave models are run with deep-water physics only, while the mesoscale model includes shallow-water physics. The global and regional versions include the assimilation of Significant Wave Height (SWH) data from the ERS-2 altimeter. A major difference between AUSWAM and other versions of WAM is that the deep-water versions of AUSWAM are run with 3rd-order propagation numerics (Bender, 1996).

Winds used to force AUSWAM are 10m surface wind velocities obtained from the Bureau of Meteorology's operational global, regional and mesoscale atmospheric models, GASP (Seaman *et al.*, 1995), LAPS (Puri *et al.*, 1998) and MESO_LAPS (National Meteorological and Operations Centre, 1999), respectively. The 10m surface winds are obtained from the lowest levels of the atmospheric models via Monin-Obukhov theory with empirical stability functions (Garratt, 1992).

### 2.1 Model Configuration

For this particular study, some details of the wave model's configuration were altered. The spatial domain is centred on Bass Strait and ranges from 45°S to 33°S and from 143°E to 155°E. Although most of the domain is more than 200m deep, the depth throughout Bass Strait is less than 80m, indicating that shallow water effects will be important in this area. The bathymetry used for this study was obtained from a 30 arc-second bathymetric dataset of the Australian continental shelf produced by the Australian Geological Survey Organisation. The spatial resolution of the wave model was increased to 0.1°, or approximately 10km. The source terms and propagation terms were integrated every 5 minutes. In terms of the wave spectrum, the directional resolution was increased to 15° while the frequency resolution remained the same as in the operational models. Fields of SWH, mean wave direction and other diagnostic variables are output every hour.

### 2.2 Wind Forcing

It is generally acknowledged that most of the errors in wave prediction fields arise from errors in the wind forcing fields (Cardone *et al.*, 1996, Komen and Smith, 1999). Therefore, for a detailed wave modelling study, it is desirable to obtain the best possible surface wind fields. In this case, they were provided by a very high resolution (0.05°) atmospheric model documented in Mills (2000). Mills (2000) shows that the hindcast is of very high quality, and we can be confident that the surface wind fields obtained from this atmospheric model are a good representation of the true conditions. This assertion will be examined more closely in Section 4.

New wind forcing fields were provided at hourly intervals. The lowest level of the atmospheric model was very close to 10m and the 10m winds were obtained in a similar way as for the operational models. Since the spatial resolution of the atmospheric model is simply twice the spatial resolution of the wave model, no interpolation of the wind fields to the wave model grid was necessary. Surface wind fields are not presented here, but the general synoptic situation was as follows.

A cold front passed through the region during the morning of December 26th, prior to the start of the yacht race. A low-pressure system formed within Bass Strait during the 26th, became cut-off at about midnight and continued to move eastwards. A small-scale secondary low developed over northern Tasmania in the early morning of the 27th, and rapidly intensified, with a band of very strong westerly winds on its northern side. It was these strong winds and the waves forced by these winds that contributed to major problems for the race fleet. A detailed description of the meteorological situation can be found in Mills (2000).

### 2.3 Boundary and Initial Conditions

To obtain boundary conditions for the Bass Strait model it was necessary to rerun the global and regional wave models with increased spectral resolution. These were forced with operational hindcast winds. The regional model provided wave spectra at 1° intervals along the edges of the high-resolution grid to use as boundary conditions.

To initialise the wave model for a cold start, JONSWAP spectra (Hasselmann *et al.*, 1973), were defined at each model gridpoint from the local initial winds according to fetch laws with a $\cos^2$ directional distribution (Gunther *et al.*, 1992). In this case, an initial fetch of 30km was imposed at all gridpoints. This ensured that some swell energy was present in the model at the beginning of the spin-up period. Initialisation for all three domains (global, regional and Bass Strait) occurred at Dec. 20th 11am (local time) and the models were spun up for 6.5 days, using the operational hindcast surface winds as forcing fields. After the initial spin-up period, the model was then run for 36 hours over the time period of interest, from Dec. 26th, 11pm until Dec. 28th, 11am.

## 3. EVOLUTION OF SWH FIELD

The predominant influence on the sea-state at any time is the local wind forcing, however there are other important elements that must be taken into consideration. In this section, three factors affecting the development of the sea-state during the yacht race are considered: 1) the wave conditions in the Tasman Sea, i.e., the area surrounding the race region, 2) the East Australian Current system and 3) the local wind forcing.

### 3.1 Tasman Sea

We first consider the wave conditions of the area surrounding the race region for the time period leading up to the yacht race. Figure 2 shows the SWH field obtained from the regional wave model at 11am on Dec. 26th, a few hours before the commencement of the race. Note that only a portion of the regional model

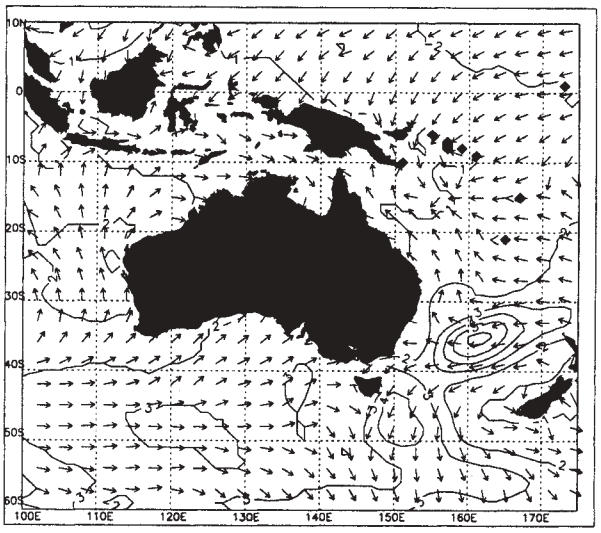


**Figure 2. SWH (m) and mean wave directions from the regional wave model at 11am on Dec. 26th, just before the start of the yacht race. An area of high SWH is present in the Tasman Sea at around (160°E, 35°S), and the mean wave directions indicate that these waves are propagating towards the Australian coast.**

domain is shown here. This figure shows that a region of high SWH has developed in the Tasman Sea, at around (160°E, 35°S) caused by strong winds associated with a low-pressure system in this area. The maximum SWH at this time is greater than 6m. The arrows on this plot represent the mean wave direction at every third model gridpoint. The mean wave direction is defined as the energy-weighted average direction of all spectral wave components. This means that if there is more than one wave system present, there may be no waves actually propagating in the 'mean' direction. However, inspection of the directional wave spectrum near the peak of this storm indicates that the vast majority of the wave energy here is propagating towards the west, with only a small directional spread.

During Dec. 27th, this area of strong winds and high SWH moves southward, while the mean wave direction turns towards the southwest. Although the area of maximum SWH remains some distance away from Bass Strait, this storm still has a significant influence over the sea-state near the coast. During the period of the yacht race, swell with a period of approximately 11 seconds propagates towards the Australian coast and into the race region.

3.2 East Australian Current

Another potentially important factor governing the development of the sea-state in the area is the East Australia Current (EAC). The EAC is a western boundary current carrying warm water from the Coral Sea southwards along the east coast of Australia. Eddies pinch off from the meanders of the EAC and the current speeds at the edge of these eddies can be up

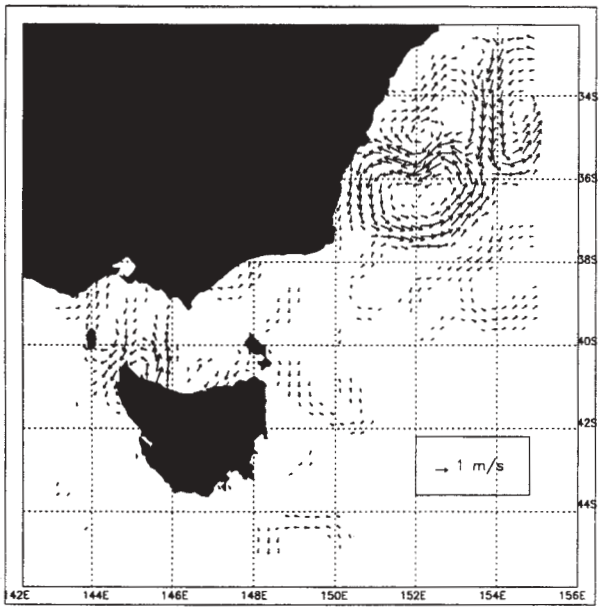


**Figure 3. Surface geostrophic currents from satellite altimetry for a 15-day time period centred on Dec. 30th 1998.**

to 2m/s (Andrews and Scully-Power, 1976). Although no direct *in situ* measurements of the velocity field of the EAC are available for the time period of the yacht race, it is possible to estimate geostrophic surface currents from satellite altimeter measurements of relative sea-surface height. Figure 3 shows surface velocities estimated from combined ERS-2 and Topex/Poseidon sea-surface height data during a 15-day time window centred on Dec. 30th, 1998. It should be noted that in depths of less than approximately 1000m, errors in correcting the observed sea-surface height for tides are too large for reliable estimates of surface currents to be made. Therefore the currents within Bass Strait are unlikely to be accurate.

It can be seen that during this time period, there was a large anti-cyclonic eddy centred at about (152°E, 36.5°S). There are strong currents around the boundary of this eddy with speeds of up to 2m/s. Note in particular an eastward-flowing current at around 37.5°S. Images of SST from infrared sensors aboard NOAA satellites confirm this diagnosis for the time period of the yacht race (G. Cresswell, personal communication).

The effect of an adverse current on a wave field is to decrease the wavelength and increase the SWH. This therefore has the effect of steepening the waves, although the amount by which the waves are altered is uncertain. Previous studies have suggested that the SWH can be increased by up to 50% in extreme cases although it is more likely to be closer to 10% (Komen *et al.*, 1994). The eastward flowing current described above will therefore cause the westerly propagating swell (from the Tasman Sea storm) to steepen.

It is currently not feasible to include the effect of surface currents in an operational wave model due to the difficulty in obtaining observed or modelled surface currents in real-time. This situation may be improved with the implementation of projects such as the Global Ocean Observing System (GOOS) or the Global Ocean Data Assimilation Experiment (GODAE) (Swail *et al.*, 1999).

3.3 Sea-state Development

It is not possible to present the entire time series of SWH fields here. A fuller description of the evolution of the sea-state can be found in Greenslade (2001). Figures 4 (a) (b) and (c) show several fields of SWH from the high resolution Bass Strait wave model during the time of interest. In Figure 4(a), a clear distinction can be seen at around 152°E between the waves propagating generally towards the southwest and waves propagating towards the east. This is the signature of the cold front passing over the area. The mean wave directions take some time to adjust to the

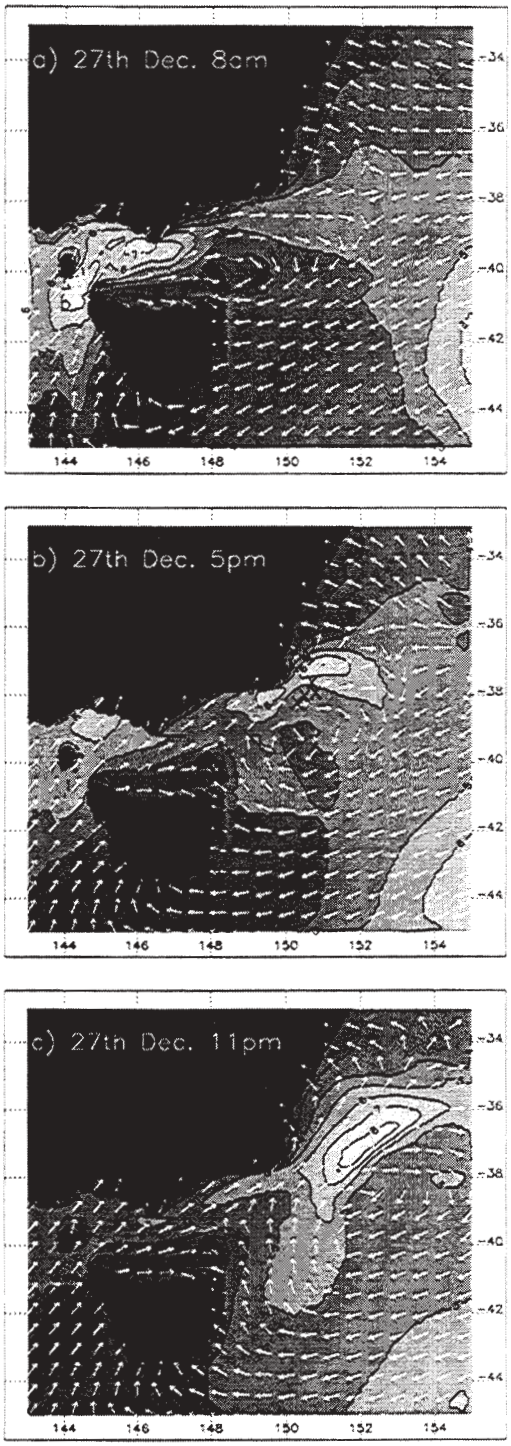


**Figure 4. SWH (m) from the high-resolution wave model. Arrows show mean wave directions. The crosses on panel (b) show the approximate locations where several of the yachts capsized or were dismasted.**

change in wind direction. The position of the 'front' in Figure 4(a) occurred in the wind field at 4am, i.e. 4 hours earlier.

After the front has swept through the Bass Strait region, the SWH in the western half of Bass Strait increases significantly, reaching a maximum of over 8m, just south of Melbourne at 11am. The mean wave direction here at this stage is towards the north, and during the afternoon of Dec. 27th, the SWH in the western half of Bass Strait abates somewhat.

The strong westerly winds associated with the small-scale secondary low pressure system over northern Tasmania cause a build-up in SWH in the eastern half of Bass Strait and by 2pm on the 27th, the SWH off the southeast corner of the continent is over 6m. By this time the passage of the low-pressure system has caused winds over most of Bass Strait to strengthen and swing to the southwest and this causes the SWH off Gabo Island to increase further (Figure 4(b)). By 11pm on Dec. 27th, the peak SWH has started to move slightly offshore (Figure 4(c)). A maximum SWH of 8.5m is reached between 10pm and 1am. During the early hours of the 28th, the area of peak SWH continues to move off into the Tasman Sea. SWH in the race region, southeast of Gabo Island remains fairly high at approximately 5m.

Figure 4(b) shows the locations where several of the yachts capsized (CYC99). These all occurred between 3pm and 7pm on Dec. 27th. It can be seen that the problems for the yachts occurred close to the area of highest SWH. However, another important consideration is the fact that multiple wave systems were present here. In particular, the easterly propagating wave systems created by the strong westerly winds combined with the westerly propagating swell arising from the earlier Tasman Sea storm, possibly steepened by the EAC. These multiple wave systems can be seen in a plot of the directional wave spectrum in Figure 5(a). This spectrum is representative of the sea-state at the second most southerly location marked in Figure 4(b). Note that the mean wave direction here is 68°, i.e., east-northeast. This is not representative of the actual sea-state, as the directional wave spectrum shows there is also a large amount of wave energy propagating towards the west.

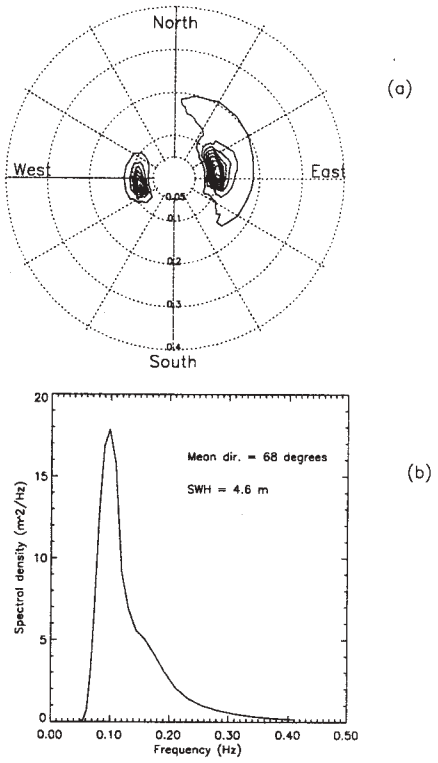


**Figure 5. (a) Directional wave spectrum ($m^2$/Hz) from the wave model at (150°E, 38.1°S) on Dec. 27th at 5pm. (b) Directional average of the spectrum shown in (a).**

The term 'crossing seas' or a 'confused sea' is used to describe the situation in which wave systems propagating in more than one distinct direction are present in a wave field. The existence of large waves propagating in many different directions causes the water surface to become highly irregular. These large, steep and chaotic waves can thus become hazardous to marine vessels. In addition, the situation depicted in Figure 5(a) shows that the 2 wave systems are propagating in almost opposite directions. Although the predominant wave direction is towards the east (the eastward peak has a higher spectral density), single waves propagating in the opposite direction will occasionally appear. These individual waves are sometimes termed 'rogue waves' (Torum and Gudmestad, 1990).

For operational purposes, marine forecasts are usually summarized in terms of SWH and mean wave direction. Further work would be required to develop techniques to summarize the sea-state when more than one wave system is significant in a region. This would need to take into account the relative significance of the superimposing wave systems and the likely impact of their combined effect on local wave characteristics.

## 4. COMPARISON WITH OBSERVATIONS

There are few reliable observations of SWH available in this area at this time - a reflection of the general difficulty in obtaining *in situ* marine observations. The locations of the ERS-2 and Topex/Poseidon satellite overpasses unfortunately do not coincide with the area of interest. We concentrate here on the data available from KFB at (148.2°E, 38.6°S) in Bass Strait (see Figure 1). In addition, some reports from the yacht fleet are considered. These, however, are subjective visual observations and are therefore less reliable than instrumented measurements.

### 4.1 Surface Winds

We first consider the accuracy of the forcing fields and compare the surface winds obtained from the atmospheric model with the observed winds at KFB. Wind speeds were measured by an anemometer mounted 44m above the sea-surface on the KFB platform. These winds need to be extrapolated to a height of 10m to enable comparison with the 10m surface winds used to force the wave model. In neutrally stable conditions, a logarithmic wind profile applies. In this particular situation, air and water temperature measurements from KFB show that after the passage of the cold front on Dec. 26th, the water was several degrees warmer than the air, resulting in low static stability. This is likely to contribute to deviations from a logarithmic wind profile. The following analysis can nevertheless provide a useful assessment of any major differences occurring between the modelled and observed surface winds.
So, assuming a logarithmic wind profile:

$$\frac{\partial u(z)}{\partial z} = \frac{u_*}{\kappa z} \qquad (2)$$

where $u(z)$ is wind speed at height $z$ above the sea-surface, $u_*$ is friction velocity and $\kappa$ is von Karman's constant (= 0.41), wind speed at 44m can therefore be converted to wind speed at 10m via:

$$u(10) = u(44) - \frac{u_*}{\kappa} \ln\left(\frac{44}{10}\right) \qquad (3)$$

Using the drag law $u_*^2 = C_D\, u(10)^2$, we find:

$$u(10) = \frac{u(44)}{1 + \frac{\sqrt{C_D}}{\kappa} \ln\left(\frac{44}{10}\right)} \qquad (4)$$

The fact that $C_D$ is itself a function of 10m wind speed again complicates these calculations, but a more detailed examination of the structure of the surface boundary layer is outside the scope of this paper. Here, $C_D$ is taken to be 0.0015, which is an appropriate value for a 10m wind speed of approximately 15m/s (Large and Pond, 1981).

Figure 6(a) shows a comparison of 10m wind speed from the atmospheric model at the location of KFB, the wind speed measured at the anemometer, and the measured wind speed extrapolated to 10m. Validation statistics are shown in the first row of Table 1.

**Table 1. Validation statistics for surface winds and SWH when compared to observations at KFB.**

| | Bias | R | *rms* | SI |
|---|---|---|---|---|
| $u_{10}$ (KFB) | -1.3 m/s | 0.58 | 3.6 m/s | 0.23 |
| $u_{10}$ (pt2) | -1.3 m/s | 0.86 | 2.7 m/s | 0.16 |
| SWH (pt2) | -0.34 m | 0.93 | 0.68 m | 0.16 |

Here, bias is (observed - modelled), *rms* is the root-mean-square difference, SI is the Scatter Index and R is the linear correlation coefficient. The SI is defined as the ratio of standard deviation of error to mean observed $u_{10}$ (or SWH) and is given by:

$$SI = \frac{\sqrt{\frac{1}{N}\sum_{i=1}^{N}\left(u_m^i - u_o^i - bias\right)^2}}{\frac{1}{N}\sum_{i=1}^{N} u_o^i} \qquad (5)$$

where $u_m$ is the modelled 10m wind speed and $u_o$ is the observed 10m wind speed.

The relatively poor match between modelled and observed wind speeds at KFB could be because the assumption of neutral stability is not appropriate in this situation. However, there is also the possibility that the small-scale features of the wind field are simply slightly displaced in the model. Upon inspection of the modelled winds from the surrounding gridpoints, it was found that the best correlation with the observations occurred at (147.8°E, 38.5°S). The 10m wind speed from this location (pt2) is shown in Figure 6(b) and the validation statistics are also shown in Table 1.

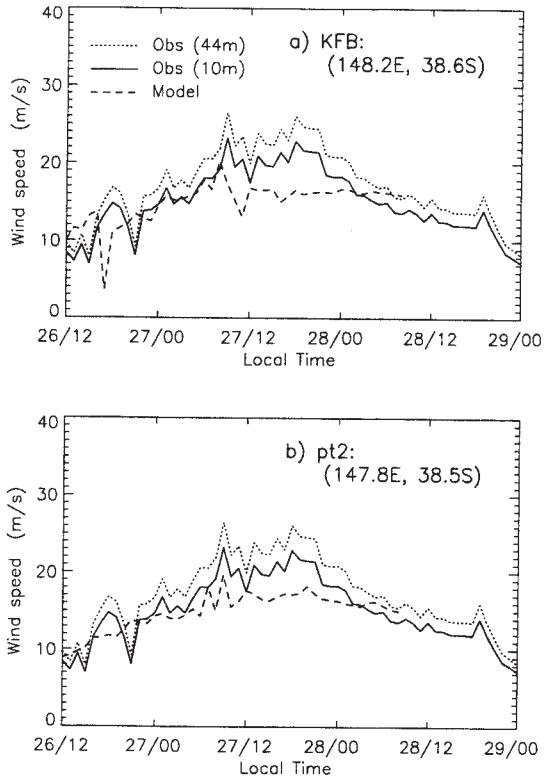


**Figure 6. (a) Comparison between 10m wind speed from the atmospheric model (dashed line) and wind speed measured by a 44m-high anemometer at Kingfish B platform (dotted line). The solid line shows the observations extrapolated to 10m assuming a logarithmic wind profile. (b) The same as (a) but modelled wind speeds are at (147.8°E, 38.5°S).**

It can be seen that although the bias is the same, there is a much greater correlation between the modelled and observed winds at this second location. This suggests that the small-scale characteristics of the wind forcing fields may be displaced slightly to the west in the atmospheric model. Following this implication, comparisons between modelled wave fields and KFB observations were performed using wave model output at this second location.

4.2 Significant Wave Height

Figure 7 shows a comparison between hourly SWH measured by a wave sensor at KFB and the SWH generated by the high-resolution wave model. Overall, there is good phase agreement between the modelled SWH and the data. The rapid increase during Dec. 27th is represented very well by the wave model, however the SWH is slightly underestimated overall, and the

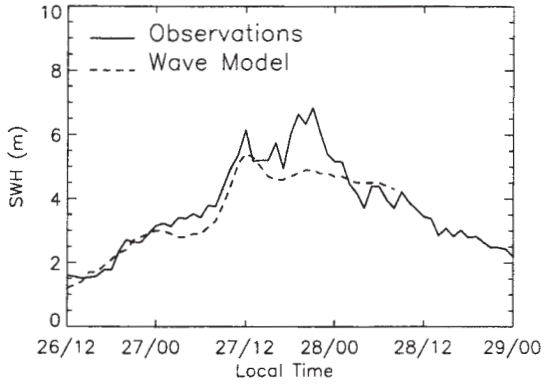


**Figure 7. Comparison between SWH from the high-resolution wave model (dashed line) and SWH measured at Kingfish B platform (solid line).**

second, larger peak is not present in the modelled SWH. In addition, the model appears to decay on a slower scale than the observations. Overall, the modelled SWH appears smoother than the observed SWH. This is to be expected as the model represents an expected value of SWH over a 10km by 10km area, rather than a value at a single location.

Validation statistics are shown in Table 1. Although the *rms* error seems high when compared to a typical operational *rms* error of about 0.4m, this is mainly due to the fact that the mean SWH here is high. The time-varying errors indicated by SI and R, show that the skill of the model in this case is very good. Note that a large portion of the bias and *rms* error here arises from the wave model not capturing the second peak in SWH. This is very similar to the pattern occurring in the wind speeds, i.e., the atmospheric model generally underpredicts wind speeds with most of the underestimation occurring during the second peak. From this, we may conclude that a large portion of the SWH bias is likely to be due to errors in the wind field.

One factor missing from the growth term within the wave model is the effect of the 'gustiness' in the wind, i.e., variability that occurs on time scales shorter than the temporal resolution of the wind fields. Generally, gusts are defined to be random wind oscillations with periods of up to 20-30 minutes. In this study, new wind fields were provided at hourly intervals and so gusts are likely to be important here. This is particularly true since this is a situation of low static stability, which implies that there will be more turbulence in the atmosphere. It has been shown that variability or gustiness in the wind speed can enhance wave growth by up to 10% (Komen *et al.*, 1994), and so this could also help explain the underprediction in the modelled SWH.

To be able to completely explain the differences between the modelled and observed SWH, it would be necessary to compare total wave spectra. This would indicate at which frequencies and in which directions the wave model is lacking in energy, i.e., whether the deficiencies are in the swell or wind-sea components of the spectrum. However, observations of wave spectra are very difficult to obtain and there were none available here during this time period.

One possible cause for underprediction of swell from the Tasman Sea storm is the 'sprinkler effect' (Booij and Holthuijsen, 1987). This is due to poor resolution in the wave spectrum and causes the disintegration of swell energy as it propagates long distances across the ocean. This can eventually result in an unrealistic spatial distribution of swell energy from distant storms. In this study, the directional resolution of the wave spectrum has been doubled from the usual operational resolution in an attempt to minimize this effect.

Another possible source of error is the lack of current or depth refraction in the wave model. It has been shown however, that depth refraction contributes very little to model performance statistics (Komen *et al.*, 1994) and it is seldom included in operational wave models. As discussed in Section 3.2, the EAC may have some effect on the development of the sea-state by steepening the westerly propagating swell arising from the Tasman Sea storm. The effects of surface currents are not included in this study. It is not clear whether the potential alteration to this swell system would still be detected at the location of the KFB platform.

4.3 Yacht Fleet Reports

CYC99 presents summaries of some visual reports from competitors made in their post-race surveys. Although highly subjective, these reports do provide some interesting information that can be useful in a general examination of the sea-surface conditions.

The average wave height reported by the fleet was 9.4m This presumably was during the worst conditions that the boats encountered, and compares fairly well with the modelled SWH of 8.5m. Assuming a Rayleigh distribution of waveheights, one might expect a maximum wave 1.91 times the SWH every 1500 waves. Assuming a peak period of 9 seconds, this would therefore be encountered on average every 3.75 hours. Most of the fleet reported that they endured the most severe conditions for at least 4 hours, so according to the wave model, it would not be unusual for individual waves of over 15m to be encountered. In fact, the average maximum wave height reported by the fleet was 14m.

The yacht fleet reported that the direction of propagation of the waves was irregular, but that the average direction was 60°. This is consistent with the modelled sea-state depicted in Section 3.3, and particularly that shown in Figure 5, where the mean wave direction is 68°. In addition, the yachts that experienced problems reported that 'exceptional' waves were responsible for causing knockdowns, and that these waves always came from a direction other than the prevailing wave pattern. This agrees with the idea of rogue waves, described previously.

Competitors in the race also commented that the 'waves had no back to them'. This effect is likely to be due to the steepening of the westerly-propagating swell by the EAC (see Section 3.2).

5. CONCLUSIONS

A high-resolution (0.1°) wave model has been run for the Bass Strait region over the period of the 1998 Sydney to Hobart yacht race. The maximum SWH reached in the wave model is 8.5m, east of Gabo Island during the evening of Dec. 27th. The model compares well with observations of Significant Wave Height (SWH) at Kingfish B Platform in Bass Strait. There is an underprediction of SWH at this location of approximately 0.34m. This is likely to be due to residual errors in the wind forcing fields. The wave model results are also consistent with visual observations of the sea-state made by competitors in the race.

Examination of the ambient sea-state conditions and directional wave spectra during the race shows that in addition to the strong winds and high SWH experienced by the fleet, there were multiple wave systems present. At times, and particularly during the peak of the storm, these wave systems were propagating in almost opposite directions. This situation is termed 'crossing seas' and has the potential to create hazardous conditions for mariners.

*Acknowledgements*
Lawson and Treloar provided the wave data from Kingfish B platform. The author wishes to thank George Cresswell for his comments on the EAC during the period of the yacht race and David Griffin for providing the gridded TP/ERS-2 surface velocity dataset. Thanks also to Rick Smith for providing the 0.1° bathymetry.

REFERENCES

Andrews, J. C. and Scully-Power, P.D. 1976. The structure of an East Australia Current anti-cyclonic eddy, J. Phys. Oc., 6, 756 - 765.

Bender, L., 1996. Modification of the physics and numerics in a third-generation ocean wave model. J. Atmos. Oc. Tech., 13, 726 – 750.

Booij, N. and Holthuijsen, L. H. 1987. Propagation of ocean waves in discrete spectral wave models, J. Comp. Phys., 68, 307 - 326.

Cardone, V.J., Jensen, R.E., Resio, D.T., Swail, V.R. and Cox, A.T. 1996. Evaluation of contemporary ocean wave models in rare extreme events: The 'Halloween Storm' of October 1991 and the 'Storm of the Century' of March 1993, J. Atmos. Oc. Tech., 13, 198 - 230.

Cruising Yacht Club of Australia. 1999. Report of the 1998 Sydney to Hobart Race Review Committee.

Garratt, J.R. 1992. The Atmospheric boundary layer, Cambridge Univ. Press, Cambridge, U.K., 316pp.

Greenslade, D.J.M. 2001. A wave modelling study of the 1998 Sydney to Hobart Yacht race, Aus. Met. Mag., (accepted).

Gunther, H., Hasselmann, S. and Janssen, P.A.E.M. 1992. Wamodel Cycle 4, DKRZ Report No. 4., Hamburg.

Hasselmann, K., Barnett, T.P., Buows, E., Carlson, H., Cartwright, D.E., Enke, K., Ewing, J.A., Gienapp, H., Hasselmann, D.E., Kruseman, P., Meerburg, A., Muller, P., Olbers, D.J., Richter, K., Sell, W. and Walden, H. 1973. Measurements of wind-wave growth and swell decay during the Joint North Sea Wave Project (JONSWAP), Dtsch. Hydrogr. Z. Suppl. A., 8(12), 95p.

Komen, G.J. and Smith, N.R. 1999. Wave and sea level monitoring and prediction in the service module of the Global Ocean Observing System (GOOS), J. Mar. Sys., 19, 235 - 250.

Komen, G.J., Cavaleri, L., Donelan, M., Hasselmann, K., Hasselmann, S. and Janssen, P.A.E.M. 1994. Dynamics and modelling of ocean waves. Cambridge University Press, Cambridge, UK, 532 pp.

Large, W.G. and Pond, S. 1981. Open ocean momentum flux measurements in moderate to strong winds, J. Phys. Oc., 11, 324 - 336.

Mills, G. A Synoptic/diagnostic study of the 1998 Sydney-Hobart yacht race storm - a warm-cored extratropical cyclone, BMRC Research Report No. 76, Bur. Met., Australia

National Meteorological Operations Centre. 1999. The operational implementation of MESO_LAPS_PT125 in NMOC, Operations Bulletin No. 49, Bur. Met., Australia.

Puri, K., Dietachmayer, G.S., Mills, G.A., Davidson, N.E., Bowen, R.A.and Logan, L.W. 1998. The new BMRC Limited Area Prediction System, LAPS, Aust. Met. Mag., 47, 203 - 233.

Seaman, R., Bourke, W., Steinle, P., Hart, T., Embery, G., Naughton, M. and Rikus L. 1995. Evolution of the Bureau of Meteorology's Global Assimilation and Prediction System, Part 1: Analyses and Initialization, Aust. Met. Mag., 44, 1 - 18.

Swail, V., Komen, G., Ryabinin, V., Holt, M., Taylor, P.K. and Bidlot, J. 1999. Wind waves in the Global Ocean Observing System, in OCEANOBS99, Proc. of the Int. Conf on the Ocean Observing System for Climate, St. Raphael, France, 1999.

Torum, A. and Gudmestad, O.T. (eds), 1990. Water wave kinematics., Kluwer Academic Publishers, Dordrecht, Holland, 771pp.